JOURNAL OF AIRCRAFT
Vol. 47, No. 1, January–February 2010

Numerical Study of Suction-Blowing Flow Control Technology for an Airfoil

P. Q. Liu,* H. S. Duan,† J. Z. Chen,‡ and Y. W. He§
Beijing University of Aeronautics and Astronautics, 100191 Beijing, People's Republic of China

DOI: 10.2514/1.45114

A new suction-blowing joint control technique is developed to reduce airfoil drag. The technique realizes suction at the airfoil leading edge and blowing at the trailing edge. As key to the difficulty of transition control, the accuracy of transition prediction under suction control is assessed by comparing the computational results with the data of a reliable experiment, and the solutions show that the corrected Wilcox transition model most accurately predicts the transition position induced by the suction. Many numerical simulations are then conducted over a range of parameters (slot width, spacing, etc.) for suction-blowing control. The physical mechanisms that govern suction and blowing drag-reduction control are determined and analyzed, and the impacts of the air mass flow rate through the slots, slot width, spacing, and size of porous region on the drag-reduction effect are discussed. Additionally, the numerical results show that suction-blowing control results in a lower drag compared with suction without blowing. The current numerical studies create a useful knowledge base for further exploration of 3-D wing suction-blowing control design.

Nomenclature

b	=	span length
C_{d0}	=	total drag coefficient without suction
C_{df0}	=	friction drag coefficient without suction
C_{dp0}	=	pressure drag coefficient without suction
C_{ds}	=	drag coefficient with suction
C_{ds-b}	=	drag coefficient with suction and blowing
C_{df-s}	=	friction drag coefficient with suction control
C_{dp-s}	=	pressure drag coefficient with suction control
C_f	=	skin friction coefficient
C_q	=	suction coefficient
c	=	chord length
D_ω	=	cross-diffusion term of turbulence dissipation frequency ω
d	=	slot width
F_2	=	blending function
G_k	=	the production of turbulence kinetic energy k
G_ω	=	production of turbulence dissipation frequency ω
k	=	turbulence kinetic energy
L	=	slot spacing
Ma	=	Mach number
n	=	number of the suction slot
Q	=	mass flow rate through the suction slot
R	=	radius of curvature
Re	=	Reynolds number based on chord length
Re_t	=	turbulence Reynolds number
S	=	strain rate magnitude
S_k	=	source terms of turbulence kinetic energy k
S_ω	=	source terms of turbulence dissipation frequency ω^i
t	=	time
U_∞	=	freestream velocity
u_i	=	velocity components
v_w	=	suction or blowing velocity through the slots
x_i	=	axes coordinates
x_{tr}	=	transition position
Y_k	=	dissipation of turbulence kinetic energy k
Y_ω	=	dissipation of turbulence dissipation frequency ω
y^+	=	boundary-layer nondimensional parameter
Γ_k	=	effective diffusivity of turbulence kinetic energy k
Γ_ω	=	effective diffusivity of turbulence dissipation frequency ω
α	=	angle of attack
α^*	=	intermittent functions
$\alpha_1, \alpha^*_\infty, \alpha^*_0, R_k$	=	constant
δ_2	=	momentum thickness of the boundary layer
δ_1	=	displacement thickness of the boundary layer
μ	=	dynamic viscosity
μ_t	=	turbulent viscosity
ρ	=	fluid density
σ_k	=	turbulent Prandtl numbers of turbulence kinetic energy k
σ_ω	=	turbulent Prandtl numbers of turbulence dissipation frequency ω
ω	=	turbulence specific dissipation rate
τ	=	wall shear stress

Subscripts

b	=	blowing conditions
i	=	1, 2 that represents x, y axes
s	=	suction conditions
∞	=	freestream flow conditions

Received 24 April 2009; revision received 29 October 2009; accepted for publication 10 November 2009.

*Professor, Institute of Fluid Mechanics, School of Aeronautic Science and Engineering; bhlpq@263.net.

†Doctoral Student, Institute of Fluid Mechanics, School of Aeronautic Science and Engineering; duanhuishen@163.com. Student Member AIAA.

‡Doctoral Student, Institute of Fluid Mechanics, School of Aeronautic Science and Engineering; cjztxh@163.com.

§Graduate Student, Institute of Fluid Mechanics, School of Aeronautic Science and Engineering; heyuwei07@163.com.

I. Introduction

DRAG reduction is one of the basic scientific and technological issues for large transport airplane development. Within the airplane's cruising drag, friction drag is an important component, especially for subsonic airplanes, with surface friction drag accounting for almost 50% of the total drag [1]. Therefore, friction drag reduction becomes a significant topic in the current airplane drag-reduction design. Furthermore, as friction drag at the turbulent boundary layer is far greater than that at the laminar boundary layer, the basic idea of friction drag reduction is focused on delaying the

occurrence of transition, expanding the range of laminar flow at the object surface, and reducing friction drag at the turbulent boundary layer. Among various drag-reduction control techniques, laminar flow control is a very effective method for friction drag reduction. It can stabilize an unstable boundary layer by inhibiting the development and amplification of various unstable disturbance waves inside the boundary layers through control measures, and accordingly, it delays the transition from laminar flow to turbulent flow at the boundary layer. Existing research works show that laminar flow control (LFC) is the most effective approach for drag reduction in large transport airplanes [2].

–The research work on LFC began in the 1930s, and it has a history of over seven decades. A number of research institutes (e.g., NASA) and researchers have carried out plenty of exploration and research work on this subject. Currently, LFC is classified into three types: laminar flow control, natural laminar control, and hybrid laminar flow control [1,3]. Laminar flow control involves suction [2], wall cooling [4], and active compliant wall technique [5], among others. Natural laminar control includes compliant wall technique [6,7], passive porous wall technique [8], and surface roughness distribution [9], among others. Hybrid laminar flow control is the combination of laminar flow control and natural laminar control, and the integration of wall shaping (with excellent pressure gradient maintained) with surface suction is currently the most popular technique. Among various control techniques, surface suction is currently the most mature and effective LFC technique, which can effectively suppress the development and amplification of all unstable disturbances, including Tollmien–Schlichting waves, crossflow instability, and attached-line instability, as well as Taylor–Görtler eddy instability [1,3]), stabilization of unstable flow, and delay in the occurrence of transition. Existing research shows that a laminar boundary layer with the highest stability can be obtained through perfect suction at a continuous porous surface. However, perfect suction is merely a concept and does not actually exist; thus, current suction control is invariably realized through surface suction with discrete holes.

Although surface suction through discrete holes can stabilize boundary layers and delay transition, this technique is very sensitive to disturbances from external factors, especially the influence of suction parameters such as hole shape, diameter, hole spacing, porosity, suction flow rate, and location of the suction zone. Even minor changes in the suction parameters can have a great effect on the stability of boundary layers [10]. Therefore, it is necessary to investigate the effect of correlative suction parameters on suction flow control before designing the LFC system and porous surface. Most existing published references are about flight tests and wind-tunnel tests concerning the impact of porous-surface suction with a fixed diameter and hole spacing on airfoil drag, whereas few are concerned with the influence of different suction parameters on boundary-layer stability, transition position, aerodynamic drag, and other factors.

Taking the previously mentioned reasons and previous research achievements into account, a numerical simulation of the diameter, hole spacing, suction area location, suction coefficient, and other suction parameters was performed. The emphasis was on the impact of suction parameters on transition position, friction drag, pressure drag, and total drag. On this basis, an active suction-blowing control technique was proposed, referring to the advantages of suction transition control and the characteristics of microblowing turbulent drag reduction [11]. To validate the application potential of this technique in drag-reduction control, the authors conducted a preliminary numerical study and investigated the influence of suction-blowing control on airfoil drag performance.

II. Computational Setup and Flow Physics Modeling

A. Turbulence Transition Model Modification

Transition position prediction is a key technique to be solved in LFC. As the wind-tunnel test requires a long period and high cost, numerical methods have gradually become the major means of transition prediction. Presently, there are many numerical methods of transition prediction. From the perspective of practical engineering application, the semiempirical e^N method and the turbulent transition model are the most frequently adopted methods of transition prediction. Owing to their short calculation period and low requirement for computer performance, they are very effective numerical methods. In the numerical calculation, the computational fluid dynamics software Fluent 6.3.26 was adopted, the shear-stress transport (SST) k-ω model was employed as the turbulent model, and the Wilcox low-Reynolds-number transition model was adopted for transition flow simulation. As the Wilcox low-Reynolds-number transition model in the SST k-ω turbulent model is sensitive to disturbances, the calculated transition position is closer to the airfoil leading edge compared with the real transition location. Therefore, it is necessary to modify the Wilcox transition model to improve the prediction precision.

The SST k-ω turbulent transport equation is as follows:

$$\frac{\partial}{\partial t}(\rho k) + \frac{\partial}{\partial x_i}(\rho k u_i) = \frac{\partial}{\partial x_j}\left(\Gamma_k \frac{\partial k}{\partial x_j}\right) + G_k - Y_k + S_k \tag{1}$$

$$\frac{\partial}{\partial t}(\rho \omega) + \frac{\partial}{\partial x_i}(\rho \omega u_i) = \frac{\partial}{\partial x_j}\left(\Gamma_\omega \frac{\partial \omega}{\partial x_j}\right) + G_\omega - Y_\omega + D_\omega + S_\omega \tag{2}$$

where G_k and G_ω are production terms of the equation, Y_k and Y_ω are dissipative terms of the equation, and Γ_k and Γ_ω are the diffusion coefficients approximated by

$$\Gamma_k = \mu + \frac{\mu_t}{\sigma_k}; \qquad \Gamma_\omega = \mu + \frac{\mu_t}{\sigma_\omega} \tag{3}$$

where μ is the laminar viscosity coefficient, and μ_t is the turbulent viscosity coefficient. With respect to the SST k-ω turbulent model, the turbulent viscosity coefficient is given by

$$\mu_t = \frac{\rho k}{\omega} \frac{1}{\max\left[\frac{1}{\alpha^*}, \frac{SF_2}{\alpha_1 \omega}\right]} \tag{4}$$

where S is the modulus of the shear strain rate, α_1 is a constant, and F_2 is a blending function used to improve the results of the turbulent viscosity coefficient in the adverse-pressure flow area on the wall. At a high Reynolds number, intermittent function α^* is equal to 1, which means the flow belongs to turbulent flow. If the influence of a low-Reynolds-number flow is considered, the Wilcox intermittent function can be expressed as follows:

$$\alpha^* = \alpha^*_\infty \left(\frac{\alpha^*_0 + Re_t/R_k}{1 + Re_t/R_k}\right); \qquad \alpha^*_0 = 0.024$$
$$Re_t = \frac{\rho k}{\mu \omega}; \qquad R_k = 6 \tag{5}$$

The turbulent model should be modified to simulate the transition flow, and a common way is to modify the expression of the intermittent function in the turbulent viscosity coefficient. As the intermittent function is merely a function of variable Re_t, only Re_t is modified and the other constants remain unchanged. It is modified according to the method presented in [12]. The modified Re_t is expressed as follows:

$$Re_t = \min\left[\frac{\rho k}{\omega \mu}, \frac{\rho k a_1}{\mu S F_2}\right] \tag{6}$$

B. Physical Model and Computational Method

For a 2-D airfoil, the suction or blowing actually occurs through infinite long slots rather than holes; hence, the slot width is used instead of the slot width in the following text. As a typical transonic airfoil, RAE2822 is chosen for the numerical calculation. As shown in Fig. 1, the region with $0 \sim 30\%$ of airfoil chord length is the suction control region, and the region with $60 \sim 90\%$ of chord length is the blowing control region. In this calculation, suction control was considered only at the upstream area of the natural transition points

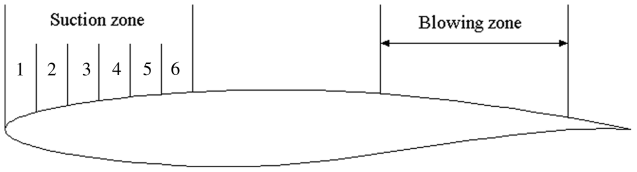

Fig. 1 Schematic suction-blowing control model for RAE2822 airfoil.

on the upper surface of the airfoil. As the natural transition positions of the airfoil vary with different Reynolds numbers, the suction region was divided evenly into six subregions. Gambit software was employed for grid generation. To simulate preferably the boundary-layer flow, the first layer grid near the wall satisfied $y^+ = 0.2 \sim 1$. Slot width was very small in comparison with the chord length of the airfoil. Therefore, to reduce the grid number and computational complexity, local refinement was done, provided that the calculation precision was maintained and conducted on the grids surrounding a slot (see Fig. 2), and the distances from the boundaries of the calculation domain to the airfoil surface were both 20 times the chord length.

Fluent 6.3.26 was used to solve the time-independent compressible-flow mass-weighted Navier–Stokes (NS) equation, energy equation, and SST k-ω turbulent model with an additional Wilcox transition model. The user-defined function program adopting language C for transition model modification was compiled and incorporated into the computational fluid dynamics (CFD) code. As the grid aspect-ratio as well as the ratio of maximum grid size to minimum size was large, double precision solver was employed to ensure stability and convergence of the numerical solution. Finite volume method was applied for equation discretization. Second-order upwind scheme was adopted for the convection terms of all solution equations, central difference scheme was used for diffusion terms, and coupled algorithm was employed for pressure-velocity coupling. The airfoil surface satisfied the nonslip boundary condition. The suction or blowing boundary was set to the mass-flow-inlet boundary condition that the mass flow rate of each slot is the same as the others, and the direction of suction or blowing flow is perpendicular to the airfoil surface. In addition, the pressure far-field boundary condition was employed for all boundaries far away from the airfoil surface.

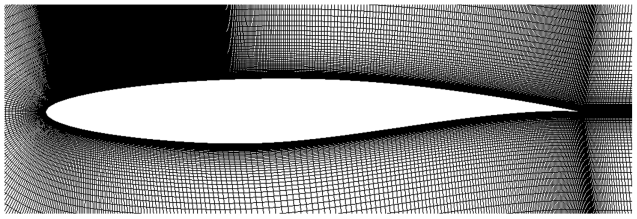

a) Grids around an airfoil

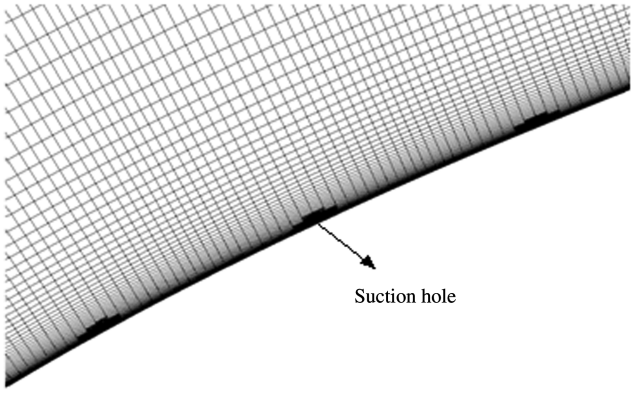

b) Partially enlarged drawing of a suction-slot grid

Fig. 2 Grids in the calculation region.

III. Numerical Results

For the convenience of result analysis and comparison, a dimensionless suction coefficient representing the mass flow rate per unit time is first defined. It is expressed as follows [13]:

$$C_q = \frac{Q}{bcU_\infty \rho_\infty} \tag{7}$$

where Q represents the mass of the inlet air passing through a suction hole per unit time, b is the spanwise length, and c is the chord length. For the 2-D airfoil, $Q = \rho_s v_s n d$ (here, ρ_s is the suction-related density, and $\rho_s = \rho_\infty$, v_s is the slot suction velocity, n is the number of suction slots, and d is the width of suction slot), and $b = 1$. Thus, Eq. (7) can be transformed to

$$C_q = \frac{n d v_s}{c U_\infty} \tag{8}$$

A. Comparison of Computational Fluid Dynamics and Experimental Results

To verify the prediction precision of the numerical results, comparison and verification analysis was conducted on the experimental values [14] and current numerical results. As shown in Fig. 3, the solid model for simulation was based on a NACA 66012 airfoil with 1 m chord but with an additional 1 m flat plate inserted at the point of maximum thickness, giving a thickness ratio of 6% and a total chord of 2 m. The suction region was within the length range of 0.47–0.77 m along the chord direction, the width of the suction slot was 0.1 mm, the slot spacing was 1 mm, and the freestream speed was 20 m/s.

Figure 4 shows the curves of the numerical results and experimental values, wherein the abscissa represents the suction coefficient (ratio of mean suction velocity to freestream velocity), and the ordinate represents the transition position increment (difference between the flow coordinates of transition position under suction control and the end of suction region). The comparison of numerical and experimental results clearly shows that the variations in transition position increments with suction coefficient are consistent with each other. Under the same suction coefficient, the transition position increments obtained in calculation and experiment fit well with one another. Accordingly, favorable calculation precision is achieved through numerical simulation, and the variation in suction-induced transition positions can be well simulated through the modified Wilcox transition model. However, the prediction of transition position displacement is not accurate enough, and it should be improved through further modification of the existing turbulent transition model.

B. Suction Impact on Airfoil Drag

As the suction-blowing control involves many control variables, some variables, for the convenience of analysis and summarization of numerical results, need to be fixed to investigate the effect of other variables on the flow control. Therefore, it is very important to obtain the minimum-drag suction coefficient when airfoil drag reaches the minimum, which can be regarded as a reference for the suction-blowing associated control.

The chord-length Reynolds numbers and Mach numbers involved in suction control calculation are 3.5×10^6 ($Ma = 0.3$) and 6.9×10^6 ($Ma = 0.6$). The angle of attack for all calculation conditions is 0 deg, the width of suction slot is $d_s = 0.1$ mm, and slot spacing is

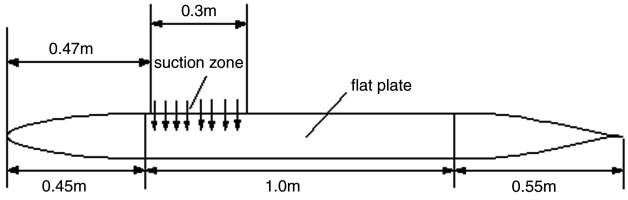

Fig. 3 Sketch of suction control for NACA66012 airfoil.

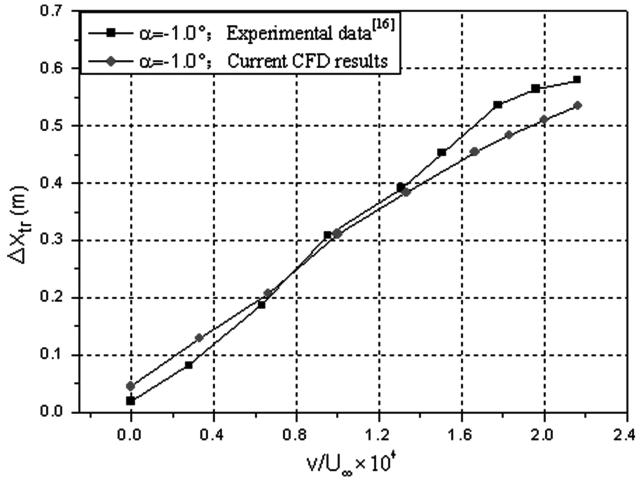

a) Transition displacement

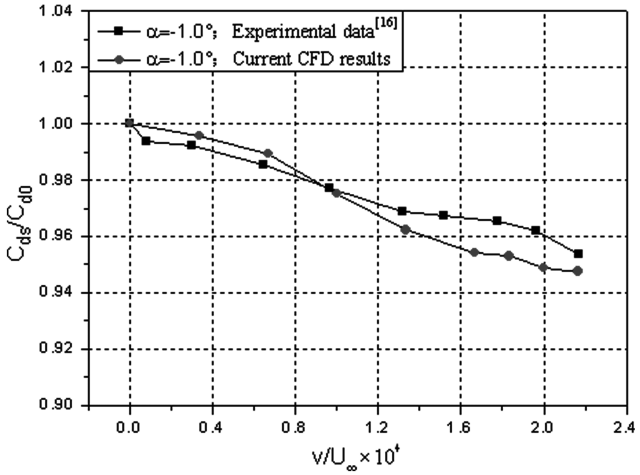

b) Drag coefficient

Fig. 4 Comparison of the computational and experimental results for suction control of the NACA66012 airfoil.

$L_s = 1$ mm, that is, 10 times the slot width [15]. For different Reynolds numbers, the natural transition positions of the airfoil upper surface as well as suction control regions are shown in Table 1.

To test for grid independence, three sets of grids with increasing grid densities (215,000, 313,000, and 423,000 computational cells labeled 1, 2, and 3, respectively) are studied. Grid refinement is considered mainly for suction slots; mesh cells of each slot are 5, 15, and 22, respectively; and mesh cells among adjacent two slots are 14, 25, and 33, respectively. These grids are studied under a Reynolds number of 3.5×10^6, and computational results for different suction coefficient are compared in Fig. 5. The differences in the computational results between set 1 and set 2, and between set 2 and set 3, are less than 1%. The relatively dense grid of set 2 is adopted in the current computation.

Figure 6 shows the variation in skin friction coefficients with suction coefficients at the upper airfoil surface, where C_f is the skin friction coefficient of the airfoil surface. Suction coefficient $C_q = 0$ means that suction control is not conducted yet. The figure indicates

Table 1 Transition positions and suction regions at different Reynolds numbers

Re	x_{tr}/c	Suction zone
3.4×10^6	27.2%	2–5
6.9×10^6	16.0%	2–3

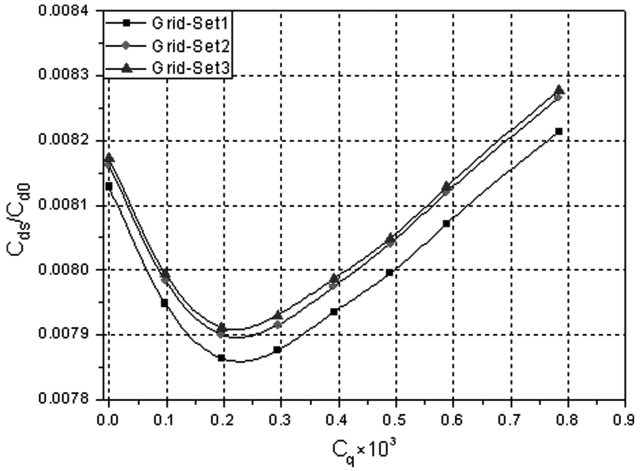

Fig. 5 Comparison of numerical results for three sets of grids.

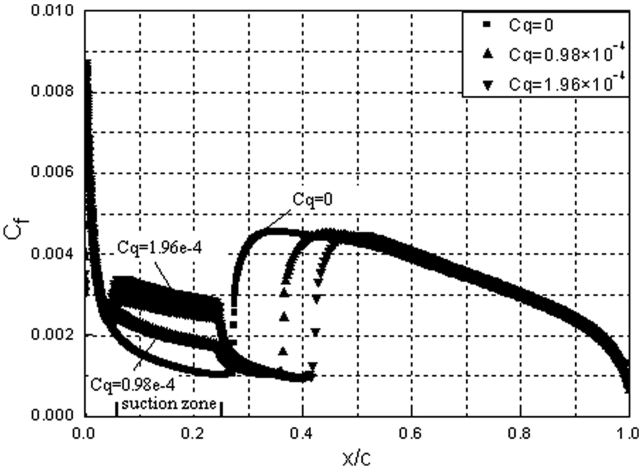

a) Re=3.4×10⁶

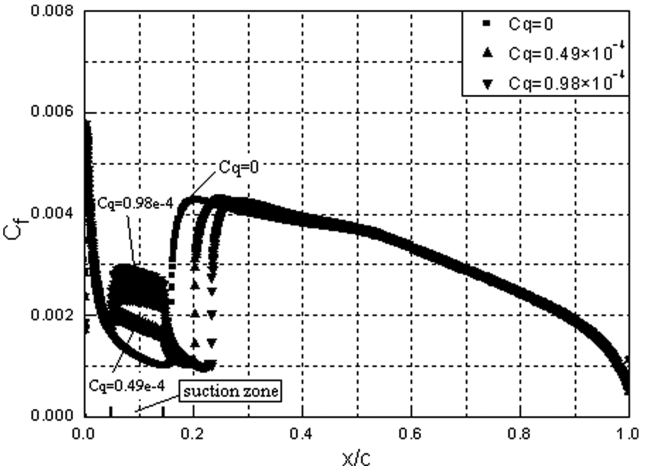

b) Re=6.9×10⁶

Fig. 6 Distribution of the skin friction coefficients on the upper airfoil surface.

that under the same Reynolds number, suction can delay the transition occurrence of upper-surface boundary layers compared with the flow of surface boundary layers without suction control. It also indicates that the transition position gradually moves toward the trailing edge with the increase of suction coefficient. Moreover, suction may cause the laminar skin friction coefficient in the suction

area to increase, which is due to the fact that surface suction causes boundary layers to be thinned and wall shearing action to be strengthened. The explanation can also be found in the following suction momentum integral equation [16]:

$$C_f = \frac{\tau_w}{1/2\rho_\infty u_\infty^2} = 2\frac{d\delta_2}{dx} - 2\frac{\rho_s \mathrm{sgn}(v_w)|v_w|}{\rho_\infty u_\infty} + 2\delta_2\left[\frac{1}{\rho_\infty}\frac{d\rho_\infty}{dx} + \frac{1}{u_\infty}\left(2+\frac{\delta_1}{\delta_2}\right)\frac{du_\infty}{dx} + \frac{1}{R}\frac{dR}{dx}\right] \quad (9)$$

Where the variable with suffix w is a physical quantity representing suction or blowing, the suffix ∞ represents the freestream conditions, R is the surface curvature radius, δ_1 is the displacement thickness of the boundary layer, δ_2 is the momentum thickness, and v_w represents the suction or blowing velocity normal to airfoil surface. The sign function of the second term at the right end of Eq. (9) can be expressed as follows:

$$\mathrm{sgn}(v_w) = \begin{cases} -1 & v_w < 0 \text{ suction} \\ 0 & v_w = 0 \\ 1 & v_w > 0 \text{ blowing} \end{cases} \quad (10)$$

Equation (10) shows that when suction is performed at the wall, the second term at the right end of Eq. (9) is positive, that is, suction can result in the increase of the skin friction coefficient, whereas conversely blowing may reduce the skin friction coefficient.

In addition, as shown in Fig. 7, the skin friction coefficient C_f of the solid surface between any two slots increases after first decreasing along the chord direction. This is caused by the fact that for the boundary-layer flow of upstream and downstream solid surface of a single suction slot, the suction effect is larger near the edge of the suction slot and is smaller farther away from the suction slot. In addition, the solid surface between the two slots is not only in the downstream of a slot but also in the upstream of another slot. Therefore, the C_f value is larger near the two ends of the solid surface between suction slots and is smaller farther away from the suction slot.

Figure 8 clearly shows that under the lower suction coefficient, the transition position takes on an approximately linear variation following the increase of the suction coefficient. As the suction coefficient continues to increase, the transition position gradually tends toward a fixed value, which is due to the small impact of surface suction on the boundary-layer stability in the downstream of suction regions. Therefore, for multiple suction regions, it is a waste to adopt a large suction coefficient for transition delay after a certain location [17].

According to the previous discussions, suction can increase the surface friction coefficient, which in turn causes the laminar friction drag in the upstream suction area of a transition point to increase. In addition, suction can delay the transition occurrence, which results in the reduction of the flow area of turbulent boundary layer, that is, turbulent friction drag decreases correspondingly. Therefore, suction can cause the laminar friction drag to increase and the turbulent friction drag to decrease. Accordingly, whether airfoil friction drag can be reduced through suction control depends on the ratio of laminar friction drag increment to turbulent friction drag decrement.

Figures 9–11 show the variations in some physical quantities with the suction coefficient. In these figures, ΔC_f represents the increment of friction drag coefficient, C_{d0} represents the total drag without suction control, and C_{ds} represents the total drag after suction control. Figures 9 and 10 indicate that under the same Reynolds number, the decrement of turbulent friction drag is equal to the

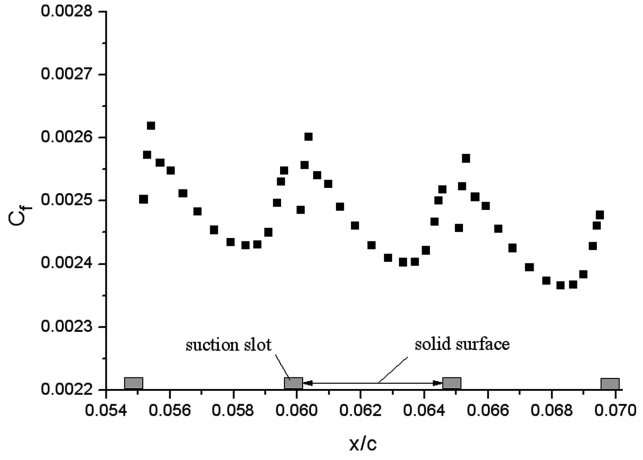

a) Re=3.4×10⁶

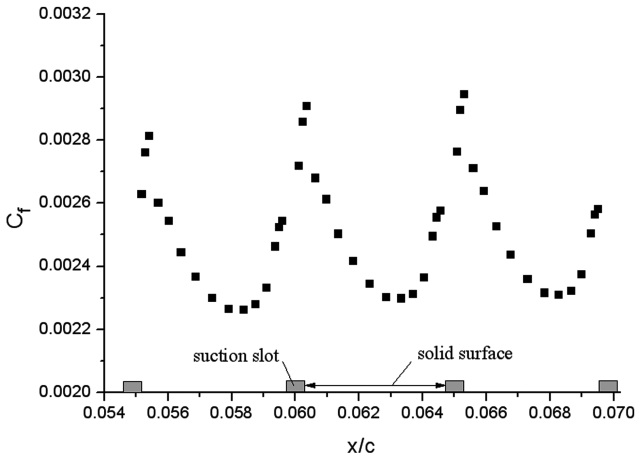

b) Re=6.9×10⁶

Fig. 7 Distribution of the skin friction coefficients between the suction holes.

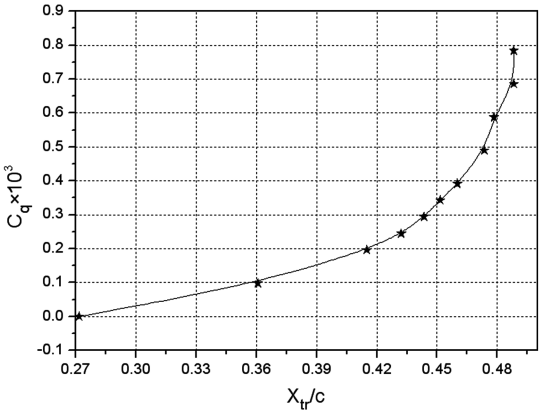

a) Re=3.4×10⁶

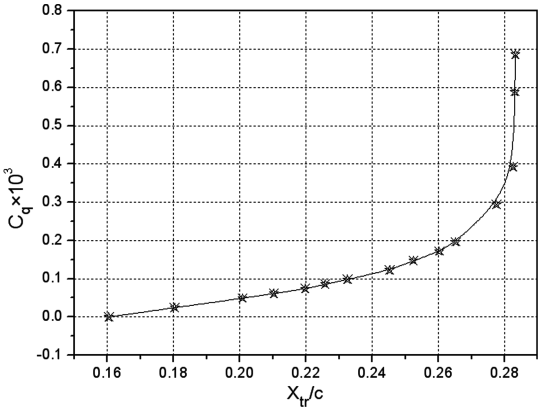

b) Re=6.9×10⁶

Fig. 8 Variation of transition position vs suction coefficient.

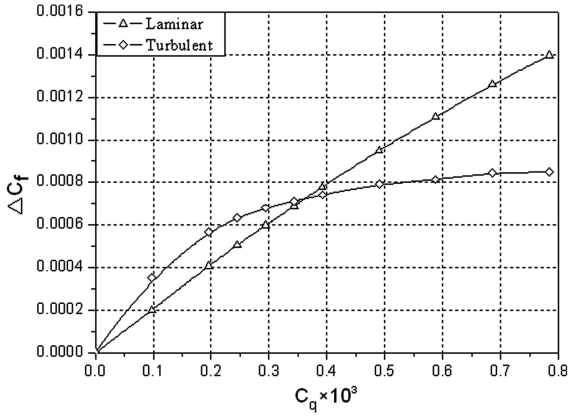

a) Re=3.4×10^6

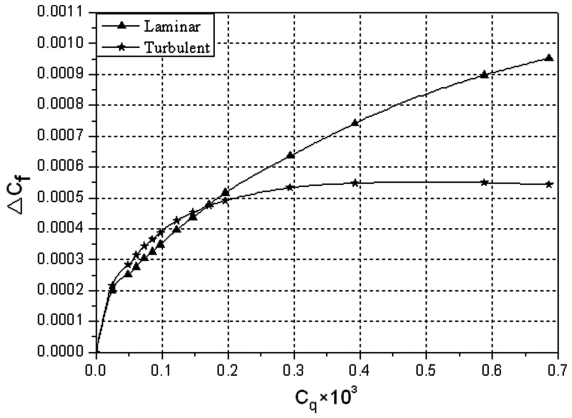

b) Re=6.9×10^6

Fig. 9 Variation in the friction drag increments of the upper-surface laminar flow and turbulent flow vs suction coefficient.

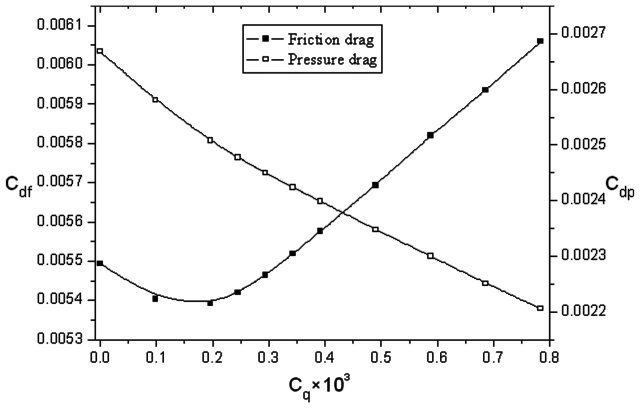

a) Re=3.4×10^6

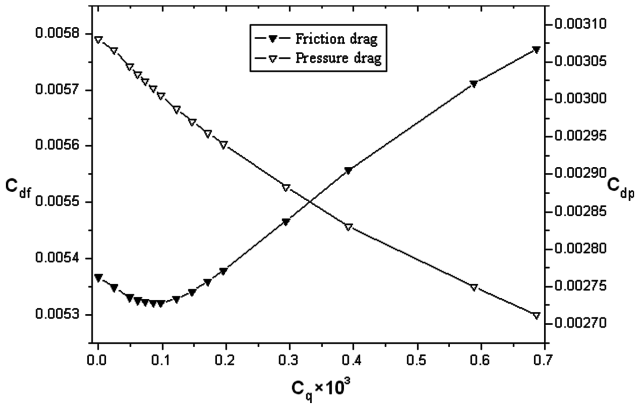

b) Re=6.9×10^6

Fig. 10 Variation in the total airfoil friction drag and pressure drag vs suction coefficient.

increment of laminar friction drag when suction coefficient is a critical value, that is, total friction drag is equal to the total friction drag without suction control. When the suction coefficient is smaller than the critical value, the decrement of the turbulent friction drag is larger than the increment of the laminar friction drag, and the total friction drag is smaller than the total friction drag without suction control, tending to increase after first decreasing to a minimum. When the suction coefficient is larger than the critical value, the decrement of the turbulent friction drag is smaller than the increment of the laminar friction drag, and the total friction drag is greater than the total friction drag without suction control, tending to increase gradually. Furthermore, the pressure drag of an airfoil decreases gradually because of the suction action, that is, the suction may cause the pressure distribution to change in the suction region. Therefore, the total airfoil drag tends to decrease after first decreasing (Fig. 11). There exists a minimum-drag suction coefficient, that is, the total drag reaches the minimum.

C. Factors Affecting Suction Control

There are many factors affecting suction control at the surface opening, of which the major ones include the geometrical parameters of a porous panel (slot shape, inner/outer slot width ratio, slot spacing, porosity, and slot depth, etc.). As for the 2-D airfoil suction control, only slot width and slot spacing are considered. In the current calculation, the flow parameters are given by $Re = 3.4 \times 10^6$ ($Ma = 0.3$). According to experimental results [18], the transition position can be delayed when the suction slot width is smaller than 0.3 mm, and the suction velocity is smaller than the maximum suction velocity that induces direct transition occurrence. Thus, the values of slot width and slot spacing should be as follows:

1) When slot spacing $L_s = 10d_s$, slot width $d_s = 0.06$, 0.1, 0.2, and 0.3 mm

2) When slot width $d_s = 0.1$ mm, slot spacing $L_s = 10$, 15, 20, 30, and $40d_s$.

1. Impact of Slot Width

The calculation results show that the variation in the suction slot widths may affect the transition position and the aerodynamic performance in suction control. It is assumed that the slot spacing L_s is equal to $10d_s$. When the suction coefficient is zero, the transition position of the upper surface for an airfoil has a small offset toward the leading edge with the increase of slot width compared with nonporous surface (see Fig. 12). This is due to the fact that the surface slot may cause the airfoil curvature to change, causing the boundary-layer flow to change as well. When the suction coefficient is not zero, the slot width impact on the transition position offset of an airfoil is also small at the same suction coefficient (Fig. 13).

In Fig. 14, the total airfoil drag follows the same trend to vary with the suction coefficient at different slot widths, that is, the airfoil drag tends to increase after first decreasing with the increase of the suction coefficient. The minimum drag under large-width suction control is relatively low, and the drag-recovery suction coefficient, which is defined as the value when the drag coefficient with the suction control is equal to the drag coefficient without suction control, grows gradually. Figures 15 and 16 show that airfoil friction drag increases after first decreasing with the increase of the suction coefficient in the same width, and the pressure drag decreases gradually. With a larger suction coefficient, the relative increment of friction drags decreases gradually with the increase in slot width. The main reason for this is that with the same suction coefficient and porosity, there are fewer slots at the suction region with large slots, which may reduce the absorption effect of the suction on the boundary-layer flow inside the

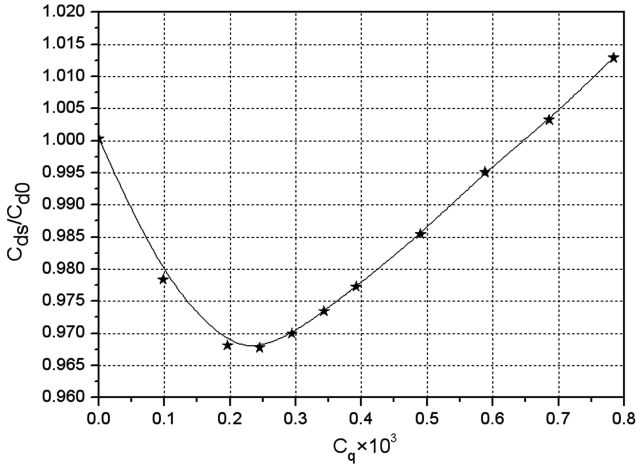

a) Re=3.4×10⁶

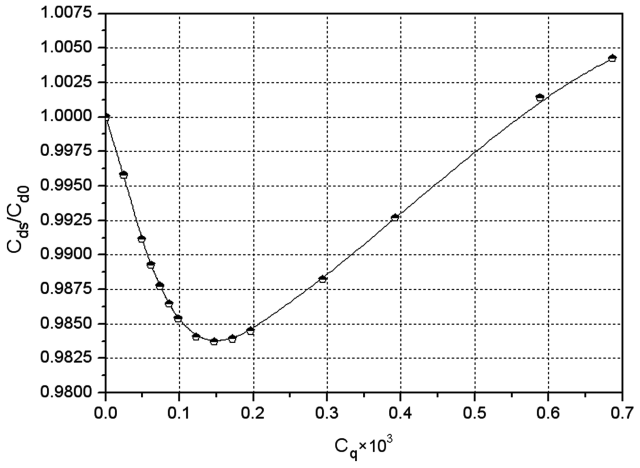

b) Re=6.9×10⁶

Fig. 11 Variation in the total airfoil drag vs suction coefficient.

suction area, subsequently reducing its influence on the wall shear stress (Fig. 17). In addition, the relative decrement of the pressure drag increases gradually with the increase of slot width; hence, the total drag decreases. Therefore, if the large slot width is adopted for suction control, the relative increment of total drag will be lower, and the drag-recovery suction coefficient will be relatively large.

2. Impact of Slot Spacing

Numerical results show that variation in slot spacing also has certain influence on airfoil suction control. As shown in Fig. 18, slot

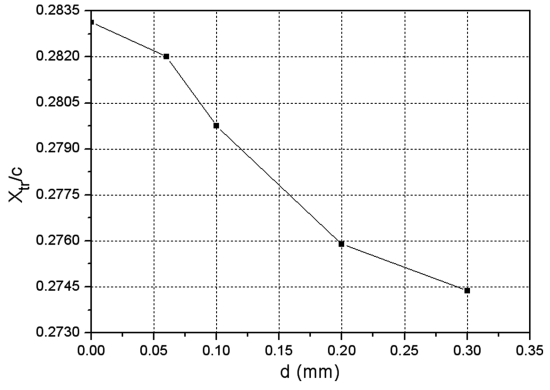

Fig. 12 Variation in transition positions on upper airfoil surface vs widths of the suction slot.

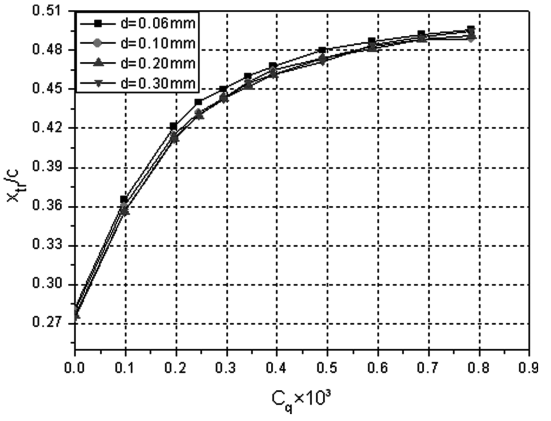

Fig. 13 Variation in airfoil transition positions vs suction coefficients at different widths.

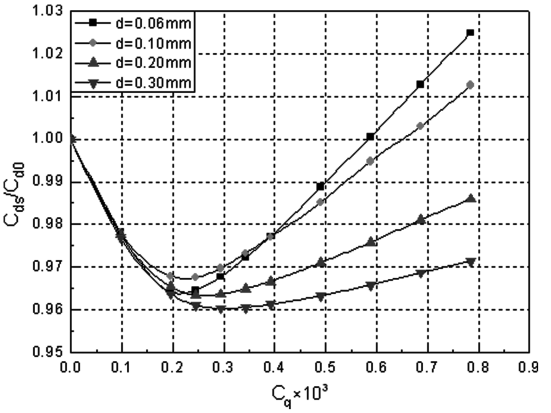

Fig. 14 Variation in airfoil drags vs suction coefficients at different slot widths.

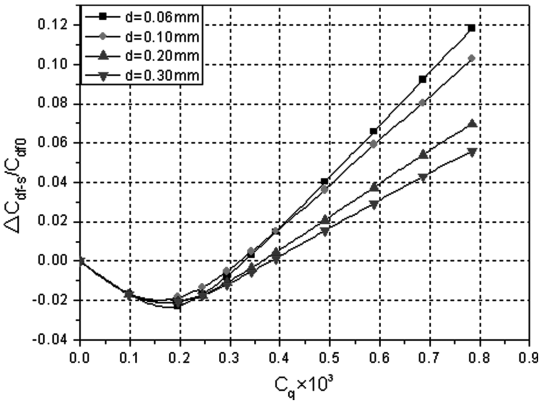

Fig. 15 Variation in airfoil friction drags vs suction coefficients at different slot widths.

spacing has a small impact on airfoil transition position at the same suction coefficient. However, slot spacing has a greater effect on total airfoil drag. Figure 19 indicates that the relative increment of total airfoil drag decreases gradually following the increase in slot spacing at a larger suction coefficient, and accordingly, the drag-recovery suction coefficient also increases. This is because the relative increment of friction drag decreases with the increase in slot spacing (Fig. 20), whereas the relative decrement of pressure drag increases (Fig. 21). Here, the main reason for the decrease in the friction drag increment is that at the same suction coefficient, the increase of slot spacing causes the porosity in the suction area to decrease, which in turn causes the region affecting the wall shear stress to shrink.

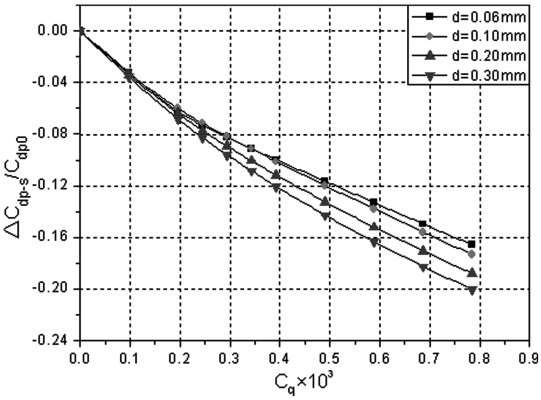

Fig. 16 Variation in airfoil pressure drags vs suction coefficients at different slot widths.

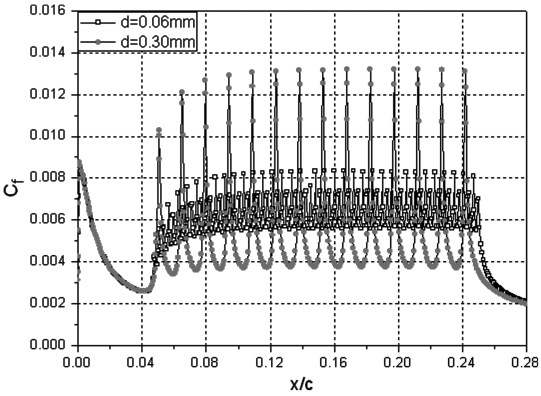

Fig. 17 Variation in airfoil upper-surface friction coefficients vs suction coefficients.

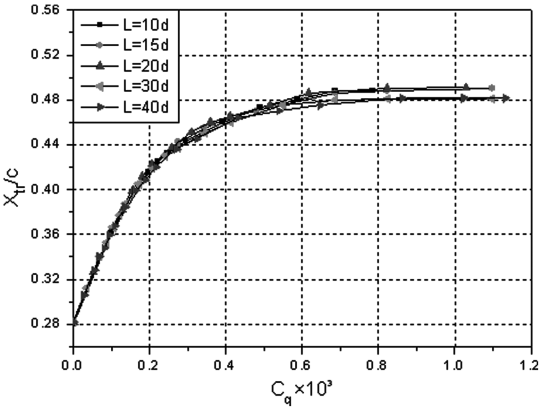

Fig. 18 Variation in airfoil transition positions vs suction coefficients at different slot spacings.

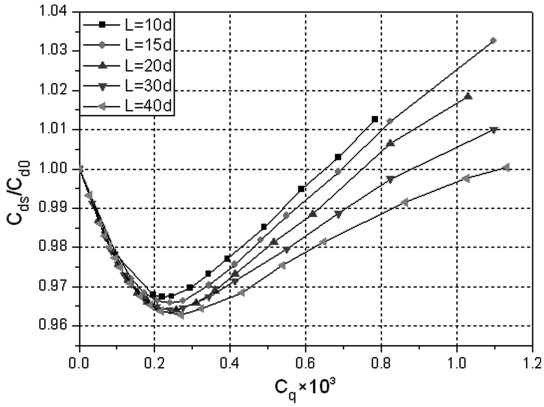

Fig. 19 Variation in airfoil drags vs suction coefficients at different slot spacings.

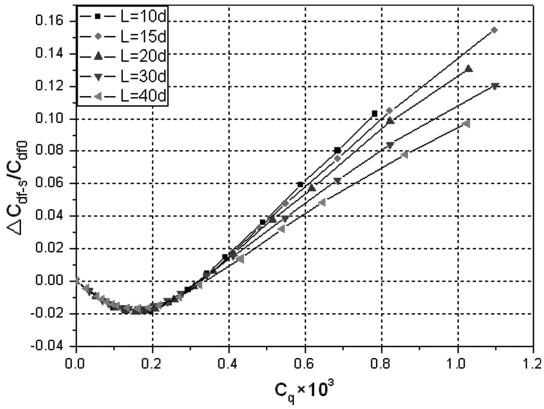

Fig. 20 Variation in airfoil friction drags vs suction coefficients at different slot spacings.

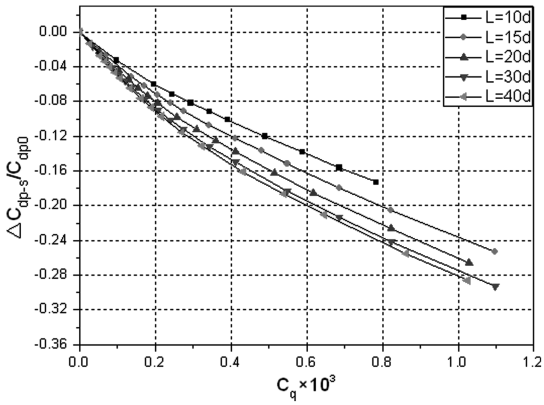

Fig. 21 Variation in airfoil pressure drags vs suction coefficients at different slot spacings.

Consequently, the shear stress at the wall near the slot edge is larger, but the shear stress at the wall among the slots is smaller (Fig. 22).

3. Impact of Suction Zone

Although the boundary-layer transition flow can be delayed effectively through surface discrete suction, the purpose of LFC is to minimize the net-drag, that is, achieving the same drag reduction with the minimum suction flow rate. By doing so, the energy consumption of the suction system and the suction momentum loss can both be reduced; thus, the net drag can be minimized. A number of factors affect the suction flow rate, among which suction distribution and suction location are two major factors. With respect to the existing studies on suction distribution optimization, the most representative ones were conducted by the research team from the University of the Southampton (United Kingdom) led by Professor Nelson, who did much theoretical and experimental work on suction optimization design [19–22]. These studies were focused on suction optimization design for plate boundary layers. An optimization algorithm was then employed in the optimized design of the suction coefficient to minimize the cost function, which is the square sum of the suction coefficients. In the current calculation, primary studies are focused on the impact of suction position. According to the definition in Sec. II.B (Fig. 1), there are several cases concerning the locations of the suction zone: 2–5 (5–25% chord length),

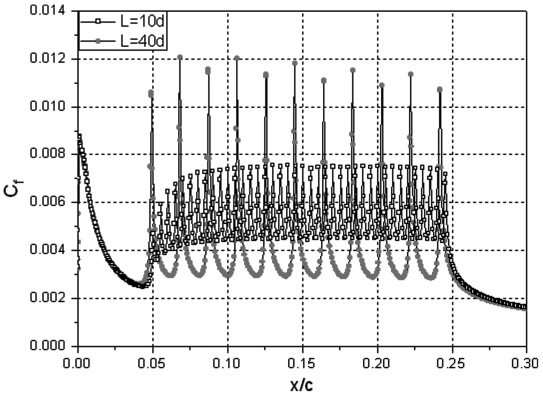

Fig. 22 Variation in airfoil surface friction coefficients vs suction coefficients at different slot spacings.

3–5 (10–25% chord length), 4–5 (15–25% chord length), and 5 (20–25% chord length). The chord-length Reynolds number and Mach number for the calculation are $Re = 3.5 \times 10^6$ $(Ma = 0.3)$, the angles of attack for all cases are 0 deg, the slot width d_s of the suction slot is equal to 0.1 mm, and the slot spacing L_s is equal to 1 mm.

Figure 23 indicates that at the same location of the suction area, the variation in airfoil transition positions with suction coefficients follows the same tendency, that is, the transition position moves backward gradually with the increase of suction coefficient, finally maintaining a fixed value. Under a medium suction coefficient $(C_q = 0.2 \sim 0.6 \times 10^{-3})$, the backward displacement of the transition position decreases gradually as the suction area becomes small. Figure 24 shows that with the shrinking of the suction area, the drag-recovery suction coefficient of an airfoil tends to increase continuously, the reason for which is that with the use of a smaller suction area and the same suction coefficient, the region affecting the wall shear stress is relatively small, leading to a lesser impact on the total friction drag. In addition, the increase of airfoil friction drag with the suction coefficient is relatively slow in the smaller suction area (Fig. 25). Moreover, with the same slot width and slot spacing, the small suction area relatively has a large reduction of pressure drag (Fig. 26).

D. Impact of Suction-Blowing Control on Airfoil Drag

Surface suction can delay the transition occurrence at the laminar boundary-layer flow and expand the laminar flow area on the airfoil surface, which will result in the reduction of the turbulent flow area so that the total friction drag becomes relatively small. However, its requirement on the surface quality is very strict. The laminar boundary-layer flow is unstable and very sensitive to external disturbances; hence, a very small object absorbed to the wall may cause a boundary-layer flow transition to occur in advance and reduce the efficiency of suction control.

To improve the drag-reduction effect of the suction control technique, the suction-blowing joint control is expected to be a high-efficiency drag-reduction control technique, which is the combination of suction laminar control and microblowing technique for turbulent drag reduction. This technique carries out suction at the leading edge and blowing at the trailing edge (Fig. 27) by installing a suction pump and a supercharging device to carry out drag-reduction control across the perforated surfaces. Thus, suction at the leading edge can be used to delay the boundary-layer transition and to expand the laminar flow area, and microblowing at the trailing edge can

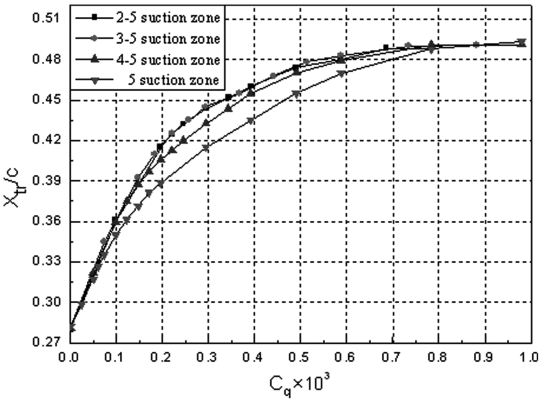

Fig. 23 Variation in airfoil transition positions vs suction coefficients with different suction areas.

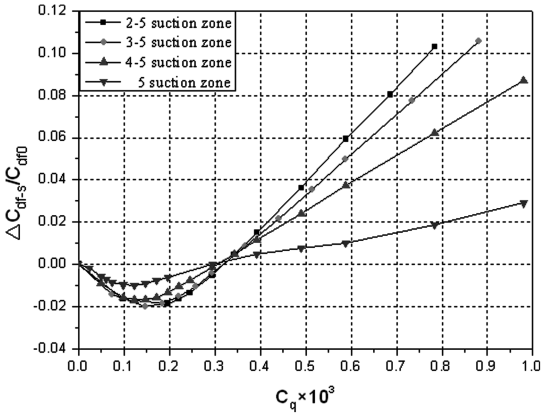

Fig. 25 Variation in airfoil friction drags vs suction coefficients with different suction areas.

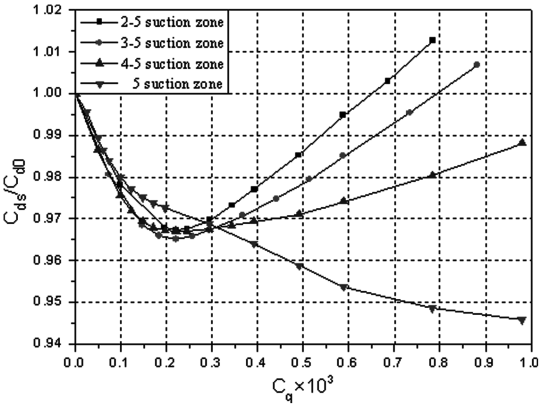

Fig. 24 Variation in airfoil drags vs suction coefficients with different suction areas.

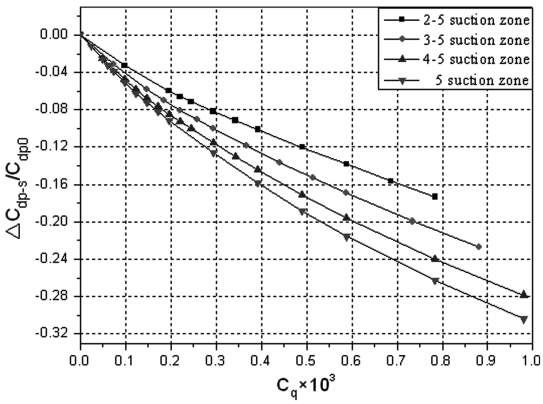

Fig. 26 Variation in pressure drag coefficients vs suction coefficients with different suction areas.

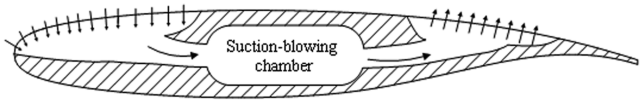

Fig. 27 Airfoil suction-blowing control scheme.

reduce turbulent friction drag by changing the surface roughness and the velocity distribution near the wall. To validate this technique, a preliminary numerical study on airfoil suction-blowing joint control was conducted.

The Reynolds number of the current numerical simulation is 3.4×10^6 ($Ma = 0.3$). The width of the suction slot and the slot spacing are the same as those mentioned in Sec. III.B, and the suction coefficient that corresponds to minimum drag is used. The blowing control area is $60 \sim 90\%$ of the chord-length range. In practical applications of the 3-D flow control, the width of the blowing slot is greater than that of the suction slot, and the column numbers of the suction and blowing slots are different. Thus, the mass flow rate of each column suction and blowing slot is different under the same total mass flow rate. Given that the mass flow rate of blowing control is d_b/d_s times larger than that of suction control, and the air velocity at the outlet of each blowing slot is the same, the impact of the width of the blowing slot and slot spacing on airfoil drag was investigated from the following two aspects:

1) With the ratio of slot spacing to slot width fixed, that is, $L_b/d_b = 10$, the width of the blowing slot was changed: $d_b = 0.1$, 0.25, 0.5, 0.75, and 1 mm.

2) With the slot spacing fixed, that is, $d_b = 0.3$ mm, the slot spacing was changed: $L_b/d_b = 5$, 10, 15, 20, and 30.

Calculation results show that turbulent friction drag can be reduced effectively through blowing, and the variation in slot width and slot spacing has a certain impact on airfoil drag. In the figure, C_{d0} represents the total airfoil drag without suction control, and C_{ds-b} represents the total airfoil drag after suction-blowing control. As shown in Fig. 28, if the air velocity at the outlet of each blowing slot is the same, L_b/d_b is equal to 10, and d_b is equal to 0.3 mm. Thus, microblowing has little impact on the transition positions at the upstream boundary layers in comparison with the cases under suction control. However, this causes the turbulent friction drag in the downstream blowing area of the transition point to decrease greatly. Therefore, the total friction drag is smaller than that under suction control.

As shown in Figs. 29 and 30, $d_b = 0$ mm represents the work condition with only suction control at the leading edge. The figures reveal that the friction drag of airfoil decreases gradually with the increase of blowing slot width. The pressure drag decreases before increasing, which is due to the fact that suction-blowing control changes the development characteristics of the boundary-layer thickness on the upper airfoil surface, consequently causing the viscosity pressure drag to change. Moreover, suction-blowing control is performed with the fixed suction flow rate, and thus the major factor affecting pressure drag is the variation in the blowing control parameters (blowing slot width and blowing velocity, etc.). The total drag tends to decrease before increasing, that is, there exists an optimal blowing slot width range ($0.2 \sim 0.5$ mm), within which the total drag of airfoil is relatively low and can be reduced by about 16%.

The previous analysis shows that under fixed slot spacing, the drag-reduction effect is better when the slot width is within 0.2 and 0.5 mm. Therefore, the blowing slot width d_b is taken as 0.3 mm to investigate the effect of slot spacing on airfoil drag performance. As shown in Fig. 31, the total airfoil drag increases gradually with the increase of slot spacing. Accordingly, the smaller the slot spacing is, the lower the airfoil drag. However, slot spacing should not be too small when surface machining, structural strength, and other factors are considered. It is also preferable for the size of the slot spacing to be around 10 times that of the slot width.

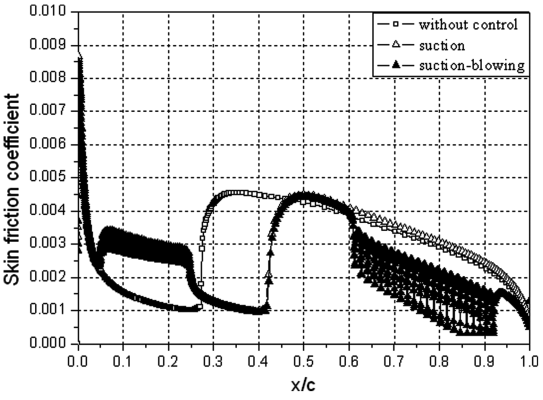

Fig. 28 Friction coefficient distribution on the upper airfoil surface under different control models.

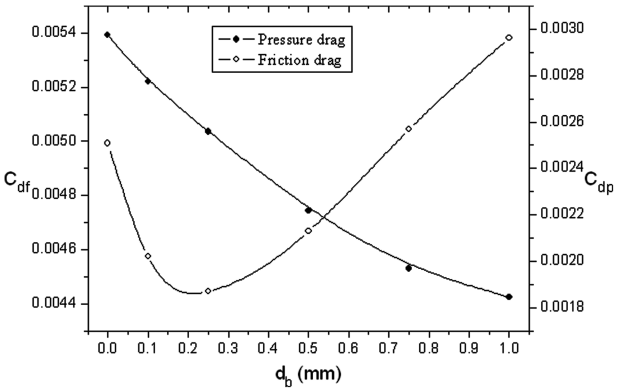

Fig. 29 $L_b/d_b = 10$, variation in total friction drag and pressure drag vs blowing slot width.

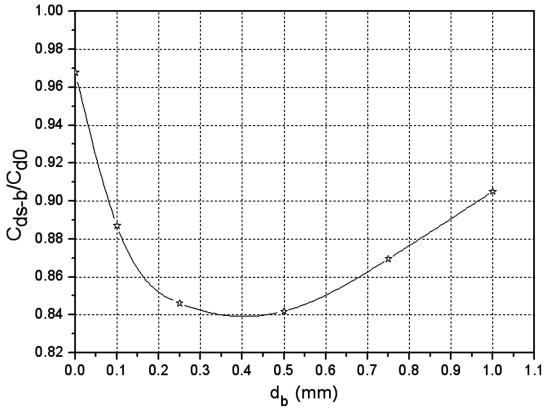

Fig. 30 $L_b/d_b = 10$, variation in total drag vs blowing slot width.

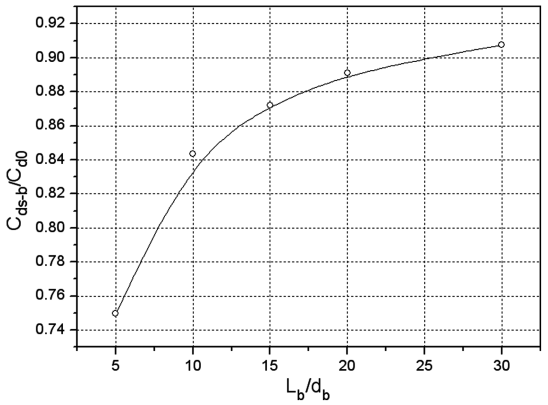

Fig. 31 $d_b = 0.3$ mm, variation in total drag vs suction slot spacing.

IV. Conclusions

In this work, we presented the numerical simulation results of suction and suction-blowing control on an RAE2822 airfoil. When several parameters (slot width, spacing, etc.) were changed over a wide range, interesting and valuable results were discovered and analyzed. The following conclusions were drawn.

1) The variation tendency of transition position induced by suction can be well simulated under the modified transition prediction model. However, the simulation of the transition position offset is still not accurate enough and needs further modification.

2) With the same slot width and slot spacing, the airfoil transition position gradually moves toward the trailing edge with the increase in suction flow rate, tending toward a fixed location.

3) The variation in both slot width and slot spacing has a certain impact on the effect of airfoil suction control. The drag-recovery suction coefficient for an airfoil may be augmented under suction control with a larger slot width and slot spacing, causing a lower minimum relative drag.

4) The smaller the suction area, the larger the drag-recovery suction coefficient becomes. The size of the suction area has lesser impact on pressure drag but has greater impact on friction drag. Furthermore, with the reduction of the suction area, its initial position gradually approaches the natural transition position, and the airfoil friction drag becomes smaller and smaller with the increase of suction coefficient.

5) At the same Reynolds number (here, $Re = 3.4 \times 10^6$), the leading-edge suction without blowing reduces the total drag below the airfoil by up to 3%, and the suction-blowing control results in a drag reduction by up to 16%.

This paper describes the 2-D airfoil suction and blowing control. For real situations, the flow is highly 3D. Based on the 3-D experimental results of suction or blowing from the published references, the surface suction can delay the boundary-layer transition position and reduce the wing drag within a certain range of suction or blowing flow rate, and the microblowing can reduce the turbulent skin friction drag in the adverse pressure gradient flow. Therefore, for real 3-D wing flow control, the suction-blowing control can also be an efficient drag-reduction technique. Although in the current numerical study only the conclusions for the 2-D airfoil suction-blowing control are given, the 2-D airfoil is a cross section of the 3-D wing, and thus the regularity of the 2-D airfoil results should be similar to that of the 3-D wing. The difference between 2-D airfoil and 3-D wing flow control is that the flow fields of the 3-D wing are highly 3D, which are subject to the impact of spanwise hole spacing and spanwise flow that leads to the difference in numerical value with 2-D airfoil results. Therefore, the results of the 2-D airfoil flow control can be considered as reference for designing the 3-D wing suction-blowing control.

Acknowledgments

The authors are grateful for the China Aviation Science and Technology Creation Funding under Grant No. 08ZA51003 and the National Basic Research Program of China (973 Program) under Grant No. 2009CB72400101. They are also grateful to the other members of their own groups for numerical performances throughout this work.

References

[1] Joslin, R. D., "Aircraft Laminar Flow Control," *Annual Review of Fluid Mechanics*, Vol. 30, No. 1, 1998, pp. 1–29. doi:10.1146/annurev.fluid.30.1.1

[2] Saric, W. S., "Laminar Flow Control With Suction: Theory and Experiment," Advisory Group for Aerospace Research and Development, Rept. 723, 1985, pp. 3.1–3.11.

[3] Joslin, R. D., "Overview of Laminar Flow Control," NASA TP-208705, 1998.

[4] Reshotko, E., "Drag Reduction by Cooling in Hydrogen-Fueled Aircraft," *Journal of Aircraft*, Vol. 16, No. 9, 1979, pp. 584–590. doi:10.2514/3.58571

[5] Zhang Qingli, Li Jingbai., "Control of Boundary-Layer Transition Control Using Active Compliant Wall Motion," *Acta Aerodynamica Sinica*, Vol. 17, No. 3, 1999, pp. 333–337.

[6] Carpenter, P. W., and Lucey, A. D., "Progress on the Use of Compliant Walls for Laminar Flow Control," *Journal of Aircraft*, Vol. 38, No. 3, 2001, pp. 504–512. doi:10.2514/2.2790

[7] Carpenter, P. W., and Morris, P. J., "The Effect of Anisotropic Wall Compliance on Boundary-Layer Stability and Transition," *Journal of Fluid Mechanics*, Vol. 218, No. -1, 1990, pp. 171–223. doi:10.1017/S0022112090000970

[8] Carpenter, P. W., and Porter, L. J., "Effects of Passive Porous Walls on Boundary-Layer Instability," *AIAA Journal*, Vol. 39, No. 4, 2001, pp. 597–604. doi:10.2514/2.1381

[9] Saric, W. S., and Carrillo, R. B., "Leading-Edge Roughness as a Transition Control Mechanism," AIAA, Reston, VA, Paper 98-16600, 1998.

[10] MacManus, D. G., and Eaton, J. A., "Measurement and Analysis of the Flow Fields Induced by Suction Perforations," *AIAA Journal*, Vol. 36, No. 9, 1998, pp. 1553–1561. doi:10.2514/2.563

[11] Hwang, D. P., "Skin-Friction Reduction by a Microblowing Technique," *AIAA Journal*, Vol. 36, No. 3, 1998, pp. 480–481. doi:10.2514/2.390

[12] Pironneau, O., and Rodi, W., *Numerical Simulation of Unsteady Flows and Transition to Turbulence*, Cambridge Univ. Press, Cambridge, England, 1992, pp. 317–373.

[13] Braslow, A. L., and Burrows, D. L., "Experimental and Theoretical Studies of Area Suction for the Control of the Laminar Flow Boundary Layer on a NACA 64A010 Airfoil," National Advisory Committee for Aeronautics, Rept. 1025, 1951.

[14] Wright, M. C. M., and Nelson, P. A., "Wind Tunnel Experiments on the Optimization of Distributed Suction for Laminar Flow Control," *Proceedings of the Institution of Mechanical Engineers, Part G: Journal of Aerospace Engineering*, Vol. 215, No. 6, 2001, pp. 343–354. doi:10.1243/0954410011533347

[15] Yong, T. M., and Humphreys, B., "Investigation of Hybrid Laminar Flow Control Surfaces," *Aircraft Design*, Vol. 4, Nos. 2–3, 2001, pp. 127–146. doi:10.1016/S1369-8869(01)00010-6

[16] Kays, W. M., Crawford, M. E., and Weigand, B., *Convective Heat and Mass Transfer*, High Education Press, Beijing, People's Republic of China, 2007, pp. 33–38 (in Chinese).

[17] Tutty, O. R., Hackenberg, P., and Nelson, P. A., "Numerical Optimization of the Suction Distribution for Laminar Flow Control," *AIAA Journal*, Vol. 38, No. 2, 2000, pp. 370–372. doi:10.2514/2.967

[18] Ellis, J. E., and Poll, D. I. A., "Laminar and Laminarizing Boundary Layers by Suction Through Perforated Plates," *Second European Forum on Laminar Flow Technology*, Association Aéronautique et Astronautique de France, Bordeaux, France, 1996, pp. 8.17–8.26.

[19] Rioual, J. L., and Nelson, P. A., "Optimum Drag Balance for Boundary-Layer Suction," *Journal of Aircraft*, Vol. 33, No. 2, 1996, pp. 435–438. doi:10.2514/3.46956

[20] Rioual, J. L., and Nelson, P. A., "Experiments on the Automatic Control of Boundary Layer Transition," *Journal of Aircraft*, Vol. 31, No. 6, 1994, pp. 1416–1418. doi:10.2514/3.46668

[21] Nelson, P. A., and Wright, M. C. M., "Automatic Control of Laminar Boundary-Layer Transition," *AIAA Journal*, Vol. 35, No. 1, 1997, pp. 85–90. doi:10.2514/2.66

[22] Veres, G. V., and Tutty, O. R., "Global Optimization-Based Control Algorithms Applied to Boundary Layer Transition Problems," *Control Engineering Practice*, Vol. 12, 2004, pp. 475–490. doi:10.1016/j.conengprac.2003.09.009